Acoustic signatures of the phase transitions in the antiferromagnet U_2Rh_2Sn

D. I. Gorbunov,[1] A. V. Andreev,[2] I. Ishii,[3] K. Prokeš,[4] T. Suzuki,[3] S. Zherlitsyn,[1] and J. Wosnitza[1,5]

[1]*Hochfeld-Magnetlabor Dresden (HLD-EMFL) and Würzburg-Dresden Cluster of Excellence ct.qmat, Helmholtz-Zentrum Dresden-Rossendorf, 01328 Dresden, Germany*
[2]*FZU Institute of Physics, Czech Academy of Sciences, Na Slovance 2, 182 21 Prague, Czech Republic*
[3]*Department of Quantum Matter, ADSM, Hiroshima University, Higashi-Hiroshima 739-8530, Japan*
[4]*Helmholtz-Zentrum Berlin für Materialien und Energie, Hahn-Meitner Platz 1, 14109 Berlin, Germany*
[5]*Institut für Festkörper- und Materialphysik, TU Dresden, 01062 Dresden, Germany*

We report on ultrasound measurements in a single crystal of the antiferromagnet U_2Rh_2Sn as a function of temperature and magnetic field. We find pronounced anomalies in the sound velocity at the Néel temperature, 25 K, and at the field-induced spin-flop-like transition at 22.5 T, which points to a strong magnetoelastic coupling. Additionally, we find that in the paramagnetic regime the temperature dependence of the magnetic susceptibility and the field dependences of the magnetization and sound velocity of transverse acoustic waves can be well described assuming a localized character of the $5f$ electrons. Using this premise, the crystal-electric-field scheme of U_2Rh_2Sn has been determined.

I. INTRODUCTION

The structural, electronic, and magnetic properties of intermetallic compounds based on uranium are widely recognized to depend on the degree of the $5f$ electron localization. The $5f$ wave functions are on the border between localized, as generally are the $4f$ states in lanthanides, and itinerant, as are the d states of transition metals, and interact strongly with their environment [1–3]. The extended character of the $5f$ states has two significant consequences. First, the defining electronic-structure quantities—the $5f$ bandwidth, the screened intraatomic f-f Coulomb interaction, and the spin-orbit interaction—are brought to the same energy scale in the eV range (the exchange interaction is usually much smaller and comparable to the external magnetic-field energy). Second, the degree of the localization of the $5f$ states is easily variable. Uranium-based compounds are strongly susceptible to variations in external parameters such as temperature, magnetic field, pressure, and elemental substitution, and can be conveniently tuned into unique electronic states.

The strong spin-orbit interaction of uranium provides significant orbital polarization of the $5f$ states and strongly couples the direction of the uranium magnetic moments and both the crystal and electronic structures. Magnetic anisotropy occurs in conjunction with elastic anisotropy: the direction of the uranium magnetic moments is determined by the bonding symmetry through a two-ion $5f$-$5f$ interaction, which, in the majority of cases, leads to extremely large anisotropy and prevalence of collinear magnetic structures [1]. The uranium moments tend to align as far as possible away from the nearest-neighbor U-U links.

Compounds with the general formula U_2T_2X (T is a d metal, X is a p metal) make it possible to test the validity of this general picture. Here, one may compare isostructural U_2Ni_2Sn and U_2Rh_2Sn. Both materials are antiferromagnets below the Néel temperature, $T_N = 25$ K [4–16]. For U_2Ni_2Sn, the U-U distances within the basal plane of a tetragonal crystal structure, 3.575 Å, are substantially shorter than those along the c axis, 3.693 Å [4,6,11]. Consequently, the magnetic moments align along the c axis [9]. For U_2Rh_2Sn, however, the shortest U-U distances, 3.586 Å, are along the c axis, while those in the basal plane are 3.622 Å [10–12]. Nevertheless, the uranium moments also align along the c axis.

U_2Rh_2Sn displays a field-induced phase transition for field applied along the easy magnetization direction [17–19]. The transition is reminiscent of a spin flop, whereby the magnetization continues to grow above the transition, showing a tendency toward saturation.

Here, we report on a high-field magnetoacoustic study of U_2Rh_2Sn. Ultrasound technique is an extremely sensitive tool for detecting magnetoelastic couplings and structural phase transitions [20,21]. Changes in the acoustic properties originate mainly from the exchange-striction mechanism as sound waves change the positions of magnetic and nonmagnetic ions and renormalize the magnetic exchange interactions. For U_2Rh_2Sn, we find pronounced anomalies in the sound velocity at the spontaneous and field-induced phase transitions. We use our experimental data to determine the crystal-electric-field scheme of this material.

II. EXPERIMENTAL DETAILS

A U_2Rh_2Sn single crystal was prepared by a modified Czochralski method as described in Ref. [12]. The lattice parameters of the tetragonal crystal structure (space group $P4/mbm$) are $a = 7.449(1)$ Å and $c = 3.586(1)$ Å. Back-scattered Laue diffraction was used to check the single-crystalline state and to orient the crystal for magnetization, specific-heat, and ultrasound measurements.

Magnetization in static magnetic fields up to 14 T was measured using a commercial physical property measurement system (PPMS). The PPMS was also used for specific-heat measurements utilizing the relaxation method.

High-field magnetization was measured in pulsed magnetic fields up to 58 T by the induction method using a coaxial pickup coil system (a detailed description of the magnetometer can be found in Ref. [22]). Absolute values of the magnetization were calibrated using data obtained in static fields.

The field and temperature dependences of relative sound-velocity changes, $\Delta v/v$, were measured using a phase sensitive pulse-echo ultrasound technique [20,21]. A pair of piezoelectric transducers were glued to opposite surfaces of the sample in order to excite and detect acoustic waves. $\Delta v/v$ is proportional to the frequency change, $\Delta \omega/\omega$, phase change, $\Delta \phi/\phi$, and sample length change, $\Delta L/L$: $\Delta v/v = \Delta \omega/\omega - \Delta \phi/\phi + \Delta L/L$. The last contribution can usually by neglected [20]. In static fields, we measured $\Delta v/v$ by fixing the phase and determining the frequency change. In pulsed fields, we fixed the frequency and analyzed the phase change of the acoustic wave.

We used Z cut and X cut LiNbO$_3$ resonant transducers (Boston Piezo-Optics Inc.) to generate and detect longitudinal and transverse acoustic waves, respectively. We measured the longitudinal, C_{11} ($k \parallel u \parallel$ [100]), C_{33} ($k \parallel u \parallel$ [001]), and transverse, C_{44} ($k \parallel$ [100], $u \parallel$ [001]), C_{66} ($k \parallel$ [100], $u \parallel$ [010]) acoustic modes. Here, k and u are the wave vector and polarization of acoustic waves, respectively. The absolute values of sound velocity for these modes at 2 K are $v_{11} = [3689 \pm 50]$ m/s, $v_{33} = [3347 \pm 50]$ m/s, $v_{44} = [1883 \pm 50]$ m/s, and $v_{66} = [1950 \pm 50]$ m/s.

III. RESULTS AND DISCUSSION

The magnetic susceptibility, $\chi = M/H$, as well as the specific heat, C, of U$_2$Rh$_2$Sn show an anomaly at $T_N = 25$ K [Figs. 1(a) and 1(b)]. The phase transition at the Néel temperature is also seen in the relative sound-velocity changes, $\Delta v/v$, due to magnetoelastic coupling [Fig. 1(c)]. The most pronounced changes at T_N are observed for the longitudinal mode C_{11} for which $\Delta v/v$ displays a step.

The magnetization, M, shows a field-induced phase transition at 22.5 T for field applied along the [001] axis at 2 K [Fig. 2(a)]. Above the transition, M changes the slope around 30 T but still continues to grow. No anomalies are observed for field applied in the basal plane. Neutron scattering shows that the uranium moments align along the [001] axis, while the rhodium moments form a noncollinear arrangement in the basal plane [12]. For isostructural U$_2$Ni$_2$Sn, the [001] axis is also the easy magnetization direction [9]. However, for field applied along this direction, U$_2$Ni$_2$Sn displays three field-induced transitions.

We measured relative sound-velocity changes for the longitudinal C_{11} and transverse C_{44} acoustic modes for U$_2$Rh$_2$Sn in pulsed fields [Fig. 2(b)]. At 2 K, $\Delta v/v$ for C_{11} shows a sharp maximum at the magnetization jump followed by a broad minimum in the field range where the magnetization changes the slope. $\Delta v/v$ for C_{44} displays a stepwise softening at the transition and changes the slope near 30 T. Pronounced
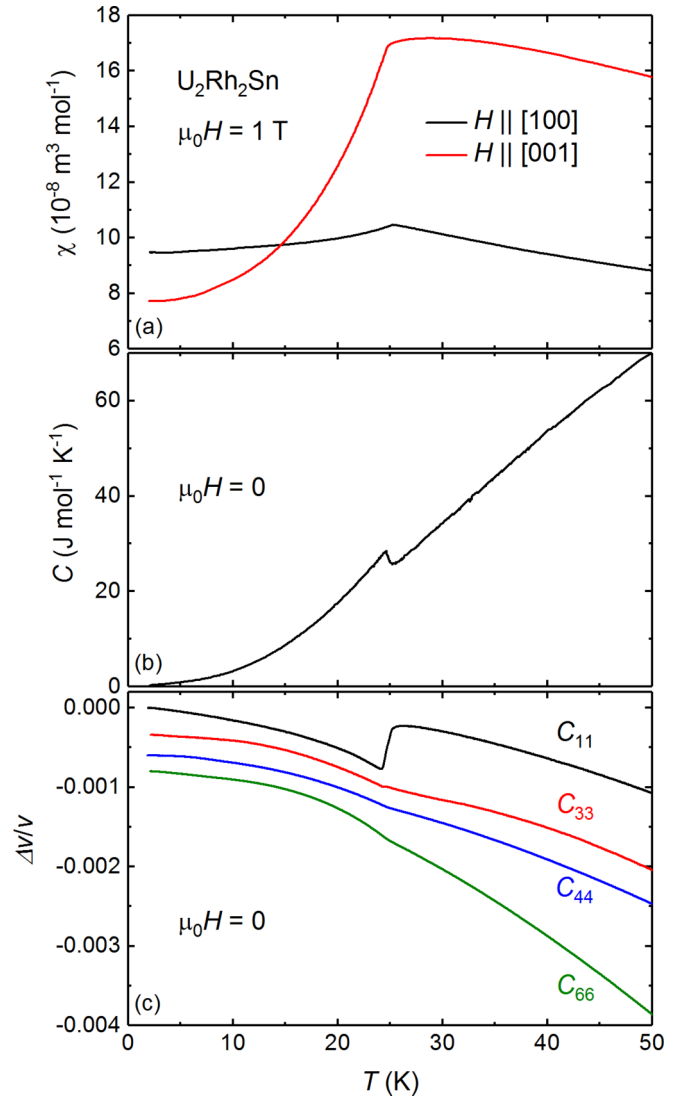

FIG. 1. Temperature dependences of (a) the magnetic susceptibility, $\chi = M/H$, in 1 T; (b) the specific heat, C; and (c) the relative sound-velocity changes, $\Delta v/v$, for the acoustic modes C_{11}, C_{33}, C_{44}, and C_{66} in zero field.

anomalies were also found in the acoustic properties at the field-induced transitions of U$_2$Ni$_2$Sn [9].

With increasing temperature, the anomaly in $\Delta v/v$ for C_{11} at the spin-flop-like transition of U$_2$Rh$_2$Sn becomes more pronounced [Fig. 3(a)]. The broader character of the anomaly at higher temperatures corresponds to a broader jump in the magnetization [12]. Above $T_N = 25$ K, the phase transition is no longer observed in $\Delta v/v$. The stepwise anomaly in the relative sound-velocity changes for C_{44} also gradually disappears with increasing temperature [Fig. 3(b)].

The magnetic phase diagram of U$_2$Rh$_2$Sn shows a good agreement between the critical fields of the spin-flop-like transition deduced from our magnetization and from the anomalies found in our sound-velocity measurements (Fig. 4).

For uranium-based intermetallic compounds, crystal-electric-field (CEF) effects are usually not so pronounced as for their lanthanide counterparts, which is due to the more extended character of the $5f$ wave functions as compared
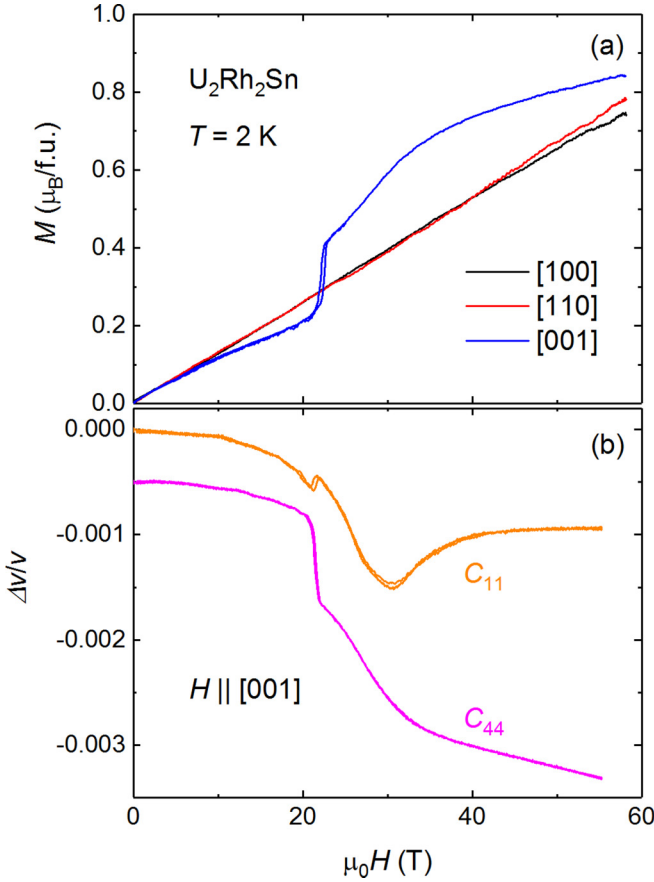
FIG. 2. (a) Magnetization, M, and (b) relative sound-velocity changes, $\Delta v/v$, for the acoustic modes C_{11} and C_{44} measured in pulsed magnetic fields up to 58 T at 2 K.

FIG. 3. Relative sound-velocity changes, $\Delta v/v$, for the acoustic modes (a) C_{11} and (b) C_{44} measured in pulsed magnetic fields up to 58 T between 2 and 30 K.

to the $4f$ wave functions. Nevertheless, some uranium-based materials show pronounced CEF effects, e.g., UNiSn and UCu$_2$Sn [23,24]. For a CEF analysis, we have to make an assumption about the state of the $5f$ electrons in U$_2$Rh$_2$Sn.

In uranium-based intermetallic compounds, the $5f$ electrons frequently show both itinerant and localized behavior, depending on the temperature [2,25]. At high temperatures the magnetic properties can be described within a localized model, whereas at low temperatures they can be explained by itinerant $5f$ electrons. U$_2$Rh$_2$Sn shows a relatively small ordered uranium magnetic moment and a small magnetic entropy [12]. This supports the picture of itinerant $5f$ electrons in the low-temperature range, below T_N. This situation likely changes at higher temperatures. One point in favor of this is that the effective magnetic moment deduced from a fit above 250 K approaches the value expected for a localized U^{3+} or U^{4+} moment [12]. We tested two U configurations for the analysis, $5f^2$ (U^{4+}) and $5f^3$ (U^{3+}), and found that the magnetic and elastic properties of U$_2$Rh$_2$Sn can be described much better by the model that assumes the $5f^2$ configuration in the paramagnetic state.

We use the CEF model to reproduce our magnetic-susceptibility, magnetization, and sound-velocity data for C_{44} [26,27]. We consider the following effective Hamiltonian:

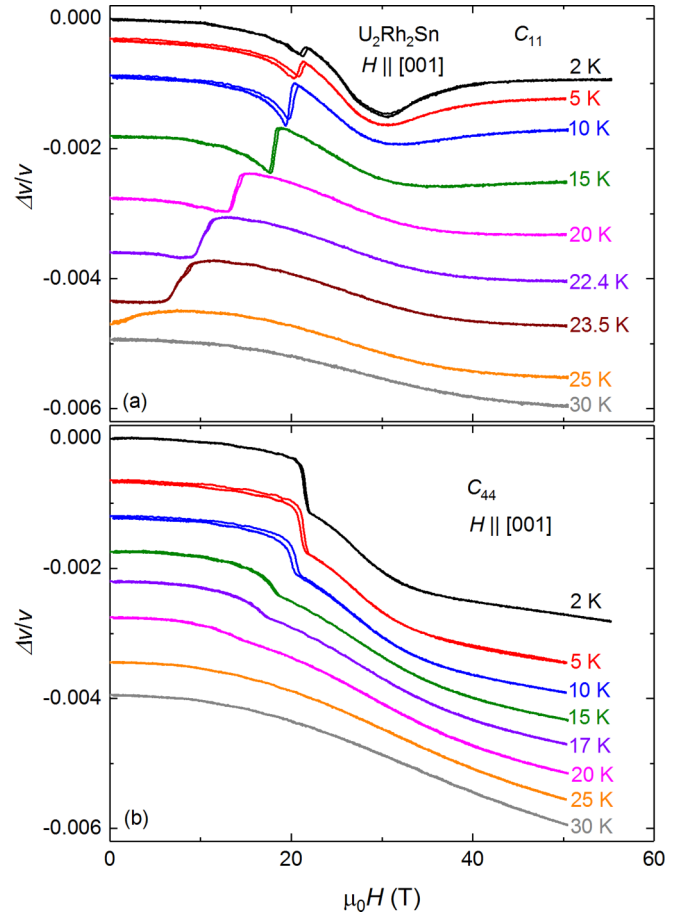$$H_{eff} = H_{CEF} + H_{sQ} + H_{QQ} + H_{Zeeman}, \quad (1)$$

where H_{CEF}, H_{sQ}, H_{QQ}, and H_{Zeeman} are the CEF, strain-quadrupole, quadrupole-quadrupole, and Zeeman energy, respectively. In the tetragonal symmetry of U$_2$Rh$_2$Sn, the CEF term is expressed as

$$H_{CEF} = B_2^0 O_2^0 + B_4^0 O_4^0 + B_4^4 O_4^4 + B_6^0 O_6^0 + B_6^4 O_6^4, \quad (2)$$

where B_m^n are crystal-field parameters and O_m^n are Stevens' equivalent operators [28]. The strain-quadrupole interaction can be expressed as

$$H_{sQ} = -\sum_i g_i O_i \varepsilon_i, \quad (3)$$

where g_i is the strain-quadrupole coupling constant, O_i is the quadrupole operator, and ε_i is the strain. Here, $i = yz, zx$ since the calculations of the elastic properties are performed for C_{44}. The quadrupole-quadrupole interaction is given by

$$H_{QQ} = -\sum_i g_i' \langle O_i \rangle O_i, \quad (4)$$

where g_i' is the quadrupole-quadrupole coupling constant and $\langle O_i \rangle$ is a thermal average of the operator O_i. The Zeeman energy is

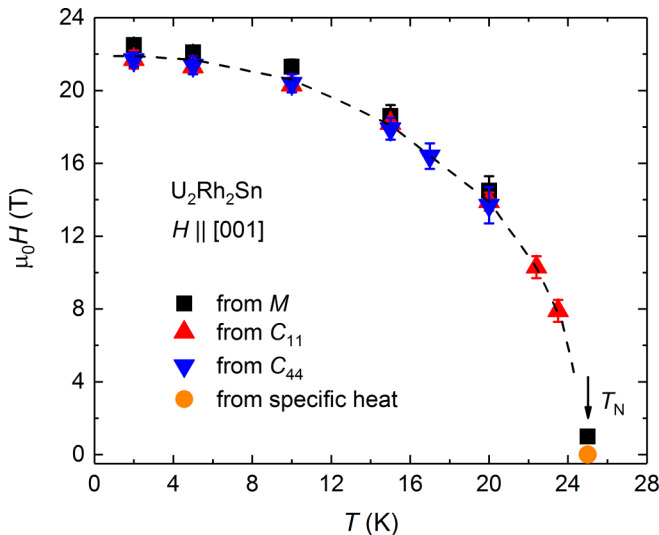$$H_{Zeeman} = -g_j \mu_B J H, \quad (5)$$

FIG. 4. Magnetic phase diagram of U_2Rh_2Sn for field applied along the [001] axis. The line is a guide to the eye.

TABLE I. CEF parameters, B_m^n (K), for U_2Rh_2Sn.

B_2^0	B_4^0	B_4^4	B_6^0	B_6^4
−39.9(5)	−0.8(5)	10.9(5)	0.1(5)	−0.5(5)

where $g_j = 0.8$ is the Landé factor and $J = 4$ is the quantum number of the total angular momentum of a U^{4+} ion.

As a first step, we tested various combinations of the crystal-field parameters assuming singlet and doublet ground states to reproduce the χ vs T and M vs H data. Then we calculated matrix elements of the nonperturbed Hamiltonian, $H_{CEF} + H_{Zeeman}$, and included quadrupolar interactions as a perturbation. This allowed us to reproduce the field dependence of the elastic modulus C_{44}. Further details of such calculations can be found, e.g., in Refs. [29,30].

The best fit of the magnetic-susceptibility data [Fig. 5(a); the chi-squared value is 21.52 for the units 10^{-8} m^3 mol^{-1}] was obtained for the crystal-field parameters listed in
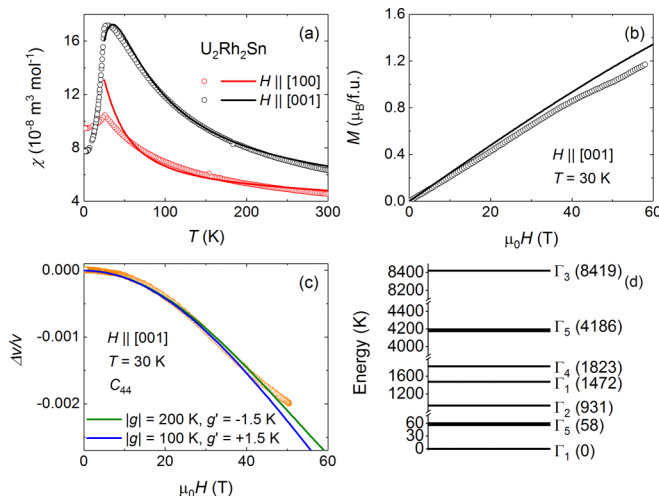

FIG. 5. (a) Temperature dependences of the magnetic susceptibility, χ; (b) and (c) field dependences of the magnetization, M, and relative sound-velocity changes, $\Delta v/v$, for C_{44}; and (d) CEF level scheme of a U^{4+} ion in U_2Rh_2Sn obtained from the CEF parameters listed in Table I. In panels (a), (b), and (c), the symbols and solid lines represent the experimental and calculated data, respectively. In panel (d), the thin lines represent singlets and the thick lines represent doublets.

Table I. We found a discrepancy between the experimental and calculated data for field applied along the [100] direction upon approaching the antiferromagnetic state for all tested combinations of the crystal-field parameters. This is likely related to changes in the localization of the $5f$ electrons with decreasing temperature. We also obtained a reasonable agreement between experiment and theory for the field-dependent magnetization at 30 K [Fig. 5(b)].

Our analysis also reproduces the elastic softening observed for C_{44} at 30 K [see Fig. 5(c) where two examples reproducing the data are shown]. Here, we varied the unknown parameters g_i between 100 and 200 K and g_i' between −1.5 and +1.5 K to obtain the best agreement with experiment. Remarkably, the use of both ferro- and antiferroquadrupolar interactions provides a satisfactory agreement with experiment. This likely indicates that quadrupole-quadrupole interactions are relatively weak but, nevertheless, have to be taken into account. Additional studies are needed to determine their role in the physics of U_2Rh_2Sn.

In a tetragonal CEF, the ninefold multiplet of a U^{4+} ion splits into five singlets and two doublets [Fig. 5(d)]. The ground state is a Γ_1 singlet and the first excited state is a Γ_5 doublet at 58 K. The next excited levels have much higher energies.

The good agreement between experiment and theory in the paramagnetic state of U_2Rh_2Sn supports the general picture of U intermetallics; namely, that the $5f$ electrons are more localized at high temperatures and more itinerant at low temperatures. In fact, this was proposed for U_2Rh_2Sn in Ref. [12] on the basis of magnetic-susceptibility data. The more localized nature of the $5f$ electrons at high temperatures leads to well-defined CEF energy levels. As the $5f$ electrons become more itinerant with decreasing temperature, a dispersion of the energy levels is likely to emerge affecting the separation between them. Here, the first excited doublet, Γ_5, at 58 K may shift to lower energies, close to 25 K, causing the phase transition at T_N.

IV. CONCLUSION

Our study revealed pronounced anomalies in the elastic properties at the spontaneous and field-induced magnetic phase transitions of U_2Rh_2Sn. We used our data to determine the crystal-electric-field scheme of this material. Our analysis shows that quadrupolar interactions have to be taken into account to reproduce the field-dependent sound-velocity data.

[1] V. Sechovský and L. Havela, Magnetism of ternary intermetallic compounds of uranium, in *Handbook of Magnetic Materials*, edited by K. H. J. Buschow, Vol. 11 (Elsevier, Amsterdam, 1998).

[2] G. Zwicknagl and P. Fulde, The dual nature of $5f$ electrons and the origin of heavy fermions in U compounds, J. Phys.: Condens. Matter **15**, S1911 (2003).

[3] J. A. Mydosh and P. M. Oppeneer, Colloquium: Hidden order, superconductivity, and magnetism: The unsolved case of URu_2Si_2, Rev. Mod. Phys. **83**, 1301 (2011).

[4] F. Bourée, B. Chevalier, L. Fournès, F. Mirambet, T. Roisnel, V. H. Tran, and Z. Zolnierek, Crystal and magnetic structures of U_2Ni_2Sn investigated by neutron diffraction and ^{119}Sn Mössbauer spectroscopy, J. Magn. Magn. Mater. **138**, 307 (1994).

[5] L. Havela, V. Sechovský, P. Svoboda, H. Nakotte, K. Prokeš, F. R. de Boer, A. Seret, J. M. Winand, J. Rebizant, J. C. Spirlet, A. Purwanto, and R. A. Robinson, Magnetism in U_2T_2X compounds, J. Magn. Magn. Mater. **140–144**, 1367 (1995).

[6] K. Kindo, T. Fukushima, T. Kumada, F. R. de Boer, H. Nakotte, K. Prokeš, L. Havela, V. Sechovský, A. Seret, J. M. Winand, J. C. Spirlet, and J. Rebizant, Electronic properties of U_2Ni_2Sn, J. Magn. Magn. Mater. **140–144**, 1369 (1995).

[7] R. P. Pinto, M. M. Amado, M. A. Salgueiro, M. E. Braga, J. B. Sousa, B. Chevalier, F. Mirambet, and J. Etourneau, Transport and magnetic properties of U_2Ni_2Sn and U_2Co_2Sn, J. Magn. Magn. Mater. **140–144**, 1371 (1995).

[8] K. Miliyanchuk, L. Havela, L. C. J. Pereira, A. P. Gonçalves, and K. Prokeš, Peculiarities of U_2T_2X hydrides, J. Magn. Magn. Mater. **310**, 945 (2007).

[9] S. Mašková, A. V. Andreev, Y. Skourski, S. Yasin, D. I. Gorbunov, S. Zherlitsyn, H. Nakotte, K. Kothapalli, F. Nasreen, C. Cupp, H. B. Cao, A. Kolomiets, and L. Havela, U_2Ni_2Sn and the origin of magnetic anisotropy in uranium compounds, Phys. Rev. B **99**, 064415 (2019).

[10] L. C. J. Pereira, J. A. Paixão, P. Estrela, M. Godinho, F. Boudarot, M. Bonnet, J. Rebizant, J. C. Spirlet, and M. Almeida, A single-crystal magnetization and neutron scattering investigation of the magnetic structure of U_2Rh_2Sn, J. Phys.: Condens. Matter **8**, 11167 (1996).

[11] H. Nakotte, A. Purwanto, R. A. Robinson, K. Prokeš, J. C. P. Klaasse, P. F. de Châtel, F. R. de Boer, L. Havela, V. Sechovský, L. C. J. Pereira, A. Seret, J. Rebizant, J. C. Spirlet, and F. Trouw, Hybridization effects in U_2T_2X compounds: Magnetic structures of U_2Rh_2Sn and U_2Ni_2In, Phys. Rev. B **53**, 3263 (1996).

[12] K. Prokeš, D. I. Gorbunov, M. Reehuis, B. Klemke, A. Gukasov, K. Uhlířová, X. Fabrèges, Y. Skourski, F. Yokaichiya, S. Hartwig, and A. V. Andreev, Anisotropic physical properties of single-crystal U_2Rh_2Sn in high magnetic fields, Phys. Rev. B **95**, 174433 (2017).

[13] M. N. Peron, Y. Kergadallan, J. Rebizant, D. Meyer, S. Zwirner, L. Havela, H. Nakotte, J. C. Spirlet, G. M. Kalvius, E. Colineau,

J. L. Oddou, C. Jeandey, J. P. Sanchez, and J. M. Winand, A new family of actinide ternary intermetallic compounds, J. Alloys Compd. **201**, 203 (1993).

[14] L. Havela, V. Sechovský, P. Svoboda, M. Diviš, H. Nakotte, K. Prokeš, F. R. de Boer, A. Purwanto, R. A. Robinson, A. Seret, J. M. Winand, J. Rebizant, J. C. Spirlet, M. Richter, and H. Eschrig, Heavy fermion behavior of U_2T_2X compounds, J. Appl. Phys. **76**, 6214 (1994).

[15] A. M. Strydom, P. de V. du Plessis, and V. V. Gridin, Low-temperature transport properties of U_2Rh_2Sn and U_2Fe_2Sn, Phys. B **225**, 89 (1996).

[16] V. H. Tran, Z. Zolnierek, A. J. Zaleski, and H. Noël, A.C.-magnetic susceptibility study of U_2T_2M (T = Ni, Rh, Pd, Ir and Pt, M = In or Sn), Solid State Commun. **101**, 709 (1997).

[17] H. Nakotte, K. Prokeš, E. Brück, N. Tang, F. R. de Boer, P. Svoboda, V. Sechovský, L. Havela, J. M. Winand, A. Seret, J. Rebizant, and J. C. Spirlet, High-field magnetization of U_2T_2X compounds (T = Co, Ni, Rh, Pd, Ir, Pt and X = In, Sn), Physica B **201**, 247 (1994).

[18] T. Fukushima, S. Matsuyama, T. Kumada, K. Kindo, K. Prokeš, H. Nakotte, F. R. de Boer, L. Havela, V. Sechovský, J. M. Winand, J. Rebizant, and J. C. Spirlet, High-field magnetization studies of some U_2T_2X compounds, Physica B **211**, 142 (1995).

[19] F. R. de Boer, K. Kindo, H. Nakotte, K. ProkešÅ¡, and V. Sechovský, U_2T_2X (T = Co, Ni, Rh, Pd, Ir, Pt; X = In, Sn) compounds in high magnetic fields, Physica B **246**, 129 (1998).

[20] B. Lüthi, *Physical Acoustics in the Solid State* (Springer, Heidelberg, 2005).

[21] S. Zherlitsyn, S. Yasin, J. Wosnitza, A. A. Zvyagin, A. V. Andreev, and V. Tsurkan, Spin-lattice effects in selected antiferromagnetic materials (Review Article), Low Temp. Phys. **40**, 123 (2014).

[22] Y. Skourski, M. D. Kuz'min, K. P. Skokov, A. V. Andreev, and J. Wosnitza, High-field magnetization of Ho_2Fe_{17}, Phys. Rev. B **83**, 214420 (2011).

[23] T. Akazawa, T. Suzuki, H. Goshima, T. Tahara, T. Fujita, T. Takabatake, and H. Fujii, Quadrupolar and magnetic phase diagram of UNiSn, J. Phys. Soc. Jpn. **67**, 3256 (1998).

[24] T. Suzuki, I. Ishii, N. Okuda, K. Katoh, T. Takabatake, T. Fujita, and A. Tamaki, Quadrupolar ordering of $5f$ electrons in UCu_2Sn, Phys. Rev. B **62**, 49 (2000).

[25] S. I. Fujimori, Y. Saitoh, T. Okane, A. Fujimori, H. Yamagami, Y. Haga, E. Yamamoto, and Y. Ōnuki, Itinerant to localized transition of f electrons in the antiferromagnetic superconductor UPd_2Al_3, Nat. Phys. **3**, 618 (2007).

[26] B. Lüthi, in *Dynamical Properties of Solids*, edited by G. K. Horton and A. A. Maradudin (North-Holland, Amsterdam, 1980), Vol. 3.

[27] N. V. Hieu, T. Takeuchi, H. Shishido, C. Tonohiro, T. Yamada, H. Nakashima, K. Sugiyama, R. Settai, T. D. Matsuda, Y. Haga,

M. Hagiwara, K. Kindo, S. Araki, Y. Nozue, and Y. Onuki, Magnetic properties and crystalline electric field scheme in RRhIn$_5$ (R: rare earth), J. Phys. Soc. Jpn. **76**, 064702 (2007).

[28] M. T. Hutchings, Point-charge calculations of energy levels of magnetic ions in crystalline electric fields, Solid State Phys. **16**, 227 (1964).

[29] D. I. Gorbunov, T. Nomura, I. Ishii, M. S. Henriques, A. V. Andreev, M. Doerr, T. Stöter, T. Suzuki, S. Zherlitsyn, and J.

Wosnitza, Crystal-field effects in the kagome antiferromagnet Ho$_3$Ru$_4$Al$_{12}$, Phys. Rev. B **97**, 184412 (2018).

[30] D. I. Gorbunov, I. Ishii, T. Nomura, M. S. Henriques, A. V. Andreev, M. Uhlarz, T. Suzuki, S. Zherlitsyn, and J. Wosnitza, Magnetic phase diagram and crystal-field effects in the kagome-lattice antiferromagnet U$_3$Ru$_4$Al$_{12}$, Phys. Rev. B **99**, 054413 (2019).

[31] http://www.mgml.eu.